

A Comparative Analysis of Single Walled CNT Bundle and Multi Walled CNT as Future Global VLSI Interconnects

Manoj Kumar Majumder, B. K. Kaushik and S. K. Manhas

Microelectronics and VLSI Group, Department of Electronics and Computer Engineering
Indian Institute of Technology, Roorkee
Roorkee, INDIA

ABSTRACT

Carbon based nanomaterials such as metallic single walled carbon nanotubes (SWNT), multi-wall carbon nanotubes (MWNT), and graphene have been considered as some of the most promising candidates for future interconnect technology. In current deep sub-micron level technology, MWNTs have potentially provided an attractive solution over SWNT bundles. This paper presents a comprehensive analysis of propagation delay for both MWNT and SWNT bundles at different interconnect lengths (global) and shows a comparison of area for equivalent number of SWNTs in bundle and shells in MWNTs. It has been observed that irrespective of the type of CNTs, propagation delay increases with interconnect lengths. For same propagation delay performance, the area occupied by SWNT bundle is more than the MWNTs for a specified interconnect length.

General Terms

Interconnect, delay, area, length, global.

Keywords

Carbon nanotube, SWNT bundle, MWNT, propagation delay, area, VLSI, nanotechnology.

1. INTRODUCTION

Continuous advances in VLSI technologies leads to development of more complex chips which contains millions of interconnections that integrate the components on the IC chip. At present VLSI technology, interconnection plays most significant role in determining the size, power consumption and clock frequency of digital system. Advancement of technological development leads for the solution of long path interconnects, which is known as global interconnects. For this global level, conventional interconnect technologies used by copper or aluminium fails because of their increasing resistivity with length which may cause some serious problems like electro migration and hillocks or voids formation in the successive levels of interconnect paths [1]. For this reason, researchers like to introduce some new materials as carbon nanotubes (CNTs) or graphene nanoribbons (GNRs) which may be a possible solution for future VLSI technologies of global interconnects.

CNTs are known as allotropes of carbon [2] and made by rolling up a sheet of graphene into a cylinder. Graphene is a monolayer sheet of graphite with sp^2 bonding of carbon atoms arranged in a honeycomb lattice structure. The sp^2 bonding in graphene is stronger than sp^3 bonds in diamond [3] which makes graphene

the strongest material. CNTs have not only unique atomic arrangement but also interesting physical properties [4]; including current carrying capability [5], long ballistic transport length [4], high thermal conductivity [6], and mechanical strength [7]. These remarkable properties make CNTs one of the most promising research materials for future VLSI technology. The extraordinary physical properties of CNTs make them exciting prospects for a variety of applications in microelectronics/ nanoelectronics [8], spintronics [9], optics [10], material science [11], mechanical [12] and biological fields [13]. Particularly, in the area of nanoelectronics, CNTs and GNRs show their prospects as energy storage devices (such as supercapacitors [14]), energy conversion devices (including thermoelectric [15] and photovoltaic [16] devices), field emission displays and radiation sources [17], nanometer semiconductor transistors [18], nanoelectromechanical systems (NEMS) [19], electrostatic discharge (ESD) protection [20], as well as interconnects [21, 22] and passives [23].

Structure of CNTs depends on chiral indices i.e., the rolling up direction of a graphene sheet. Depending on the chiral indices (n, m), CNTs can get their unique armchair or zigzag structures. For armchair CNTs, the chiral indices is defined by $n = m$ [3] and for zigzag CNTs, it is n or $m = 0$ [3]. For other values of n and m , CNTs are known as chiral. Depending upon their different structures, CNTs can exhibit both metallic and semiconducting properties. By satisfying the condition $n - m = 3i$ (where i is an integer), armchair CNTs are always metallic and zigzag CNTs are either metallic or semiconducting in nature depending on their chiral indices [3, 4]. Statistically, a natural mix of CNTs will have $1/3^{\text{rd}}$ of metallic and $2/3^{\text{rd}}$ of their semiconducting chirality [24]. These unique structures of CNTs basically depend on the rolling up directions of graphene sheet. CNTs are also classified into single-walled nanotubes (SWNTs) and multi-walled nanotubes (MWNTs). The main difference between SWNT and MWNT arises from number of concentrically rolled up graphene sheets. For SWNTs, only one rolled up graphene sheet is there whereas for two or more concentrically rolled up graphene sheets, CNTs are known as MWNT. SWNT bundle is formed by packing together a large number of SWNTs in a bundle form. The parasitic elements of SWNT bundle and MWNTs depend on number of metallic SWNTs in the bundle and number of shells in the MWNTs. It is very difficult to achieve ballistic transport for MWNTs for a long length whereas SWNTs have mean free path of the order of a micron [25] due to its diameter in nano range.

The paper is organized as follows. In section 2, different interconnect models of SWNT bundle and MWNT are reviewed. Section 3 introduces simulation setup for calculating propagation delay on the basis of described models in section 2. Graphical plots of propagation delay for MWNT shells with equivalent numbers of SWNTs in bundles at different global interconnects lengths are presented in section 4. Finally, section 5 draws a brief summary.

2. INTERCONNECT MODELS OF SWNT BUNDLE AND MWNTS

Depending on different interconnect parasitics such as resistance, capacitance and inductance, *RLC* circuit models for both MWNT and SWNT bundle interconnects are presented [26, 27] on the basis of semi-classical one-dimensional electron fluid model [28, 29]. This 1-D electron fluid model is derived from a classical two-dimensional electron fluid theory [4, 30] taking into account electron-electron repulsive force.

2.1 Model of MWNT Interconnect

MWNTs have diameters in a wide range of a few to hundreds of nanometers. It has been shown that all shells of MWNT can conduct if they are properly connected to contacts [31-33] and the contact resistance gets much lower value than SWNTs. Naemi et al. [34] shown that the conductivity of MWNTs are several times larger than that of Cu or SWNT bundles for long lengths of interconnects which is generally defined as global interconnects.

MWNTs have different number of shells. The number of metallic shells in a MWNT can be calculated as [27],

$$M = \beta \left[1 + \frac{D_I - D_N}{2\delta} \right] \quad (1)$$

where D_I and D_N are the outermost and innermost shell diameters of MWNT, respectively. δ is the spacing between shells in a MWNT and the value is defined as $\delta = 0.34$ nm [26]. The square bracket term of equation (1) is a floor function and the factor β is the ratio of metallic shells to those shells in a MWNT. When $D_I \leq 10$ nm [27], then one-third of the shells are metallic and rest of the shells are semiconducting. However, for $D_I > 10$ nm, β increases due to interaction between adjacent shells for the MWNT.

The *RLC* model of a metallic MWNT interconnect is shown in Figure 1. In this model [27], magnetic inductance is neglected compared with kinetic inductance as the value of magnetic inductance is much smaller than kinetic inductance for a CNT [25]. Kinetic inductance comes from the kinetic energy of electrons which comes from the classical definition of current equation [4]. Therefore, kinetic inductance per unit length is formulated by approximating the kinetic energy per unit length of a 1-D wire [3, 4, 29] and expressed by the equation

$$L_K = \frac{h}{2e^2 v_F} \quad (2)$$

where h is the plank's constant, e is electron charge and v_F is the Fermi velocity of graphene ($= 8 \times 10^5$ m/s). Therefore, value of kinetic inductance of a CNT is given by 16 nH/ μm [25]. Due to

band structure, SWNT has two propagating channels and for each channel, electrons have the properties of spin up and spin down [4]. For this fourfold band degeneracy, kinetic inductance per unit length is arrived as 4 nH/ μm [35].

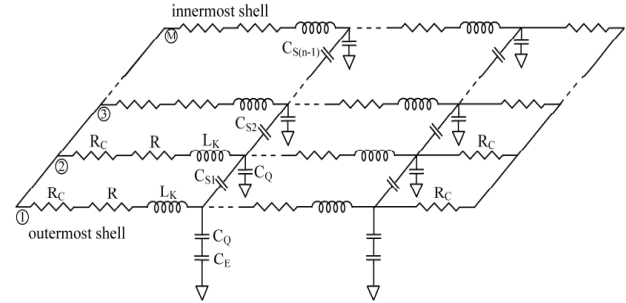


Fig 1: *RLC* circuit of a metallic MWNT interconnects [27].

In the given model of Figure 1, electrostatic capacitance (C_E) does not exist in inner shells of MWNTs as outermost shells of MWNTs shield inner shells from the ground plane. However, quantum capacitance (C_Q) exists at each sheet of MWNTs which is defined from the quantum classical theory and can be expressed as [29],

$$C_Q = \frac{2e^2}{h v_F} \quad (3)$$

However, an additional electrostatic capacitance (C_S) exists between the neighboring metallic shells, which can be formulated as,

$$C_S = \frac{2\pi\epsilon_0}{\ln\left(\frac{D_i}{D_j}\right)} \quad (4)$$

where ϵ_0 is the permittivity of the vacuum, D_i and D_j are the diameters of the i^{th} and j^{th} metallic shells, respectively and $i < j$.

The circuit model presented in Fig.1 is simplified in Figure 2 by considering identical inner shells of MWNTs. In this simplified model presented in Figure 2, it is assumed that the outershell of MWNT is metallic. There are no variation in distributed parameters, R and L_K as they are same for each shell of MWNT. Now, by assumption of equal potential across components of each shell in a MWNT, the circuit model of Figure 2 is again simplified to an equivalent circuit model which is presented in Figure 3. In this simplified model of Figure 3, it is again considered that the *RLC* parts of all inner shells are identical. For all the circuit models presented in Figs [1-3], R_C is the contact resistance and its ideal value is defined as 3.2 K Ω per shell [26]. The values of C_E and C_Q are of the same order. C_Q appears in parallel for all metallic sheets with a series combination of C_E . Therefore, for M number of metallic sheets C_Q appears as ($M \times C_Q$) and the value of C_E appears as in the previous case.

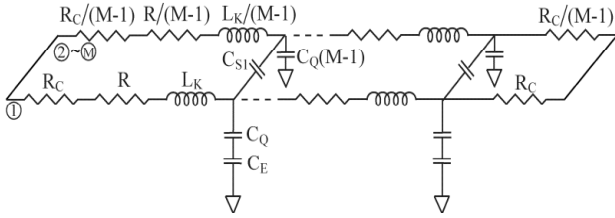


Fig 2: Simplified equivalent circuit of a metallic MWNT interconnects [27].

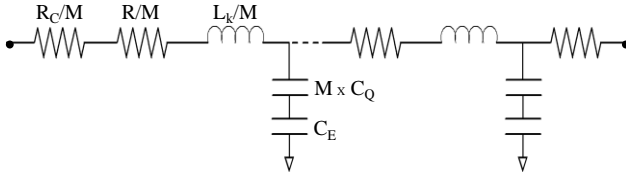


Fig 3: Simple equivalent circuit model of a metallic MWNT interconnects [27].

2.2 Model of SWNT Bundle Interconnect

The *RLC* model of SWNT bundle [27, 36] considers all individual SWNTs at parallel directions in the bundle. The spacing between SWNTs in bundle is determined by vander waals forces between the atoms in adjacent nanotubes. The metallic nanotubes are distributed randomly with a probability $\beta=1/3$ due to lack of chirality [27]. The proportions of metallic nanotubes are therefore potentially be increased using techniques reported in [37] and [38]. Therefore, total number of metallic SWNTs is formulated as shown in Fig. 4 [27],

$$N = \beta \left[N_x N_y - \left[\frac{N_y}{2} \right] \right] \quad (5)$$

where N_x and N_y are number of SWNTs in the bundle at horizontal and vertical directions, respectively. The distance between adjacent SWNTs in bundle can be derived from cross-section of a bundle (Figure 4) as [27],

$$d_b = \delta + d \quad (6)$$

where $\delta = 0.34$ nm is the spacing between SWNTs in the bundle and d is diameter of SWNT. The equivalent circuit of SWNT bundles interconnect is shown in Figure 5, where N_a and N_b denote number of upper level and bottom level SWNTs (Figure 4) [27].

For *RLC* model of SWNT bundle presented in Figure 5, the assumption is made for all SWNTs in the bundle are identical and each SWNT has same potential across it [27]. The equivalent circuit of Figure 5 is further simplified in Figure 6, where electrostatic capacitance between neighboring metallic SWNTs (C_b) has no effect on circuit behavior and $(\beta N_x \times C_E)$ can be regarded as an electrostatic capacitance between SWNT bundle and ground plane. In upper level of SWNTs, C_E does not exist as bottom level shields the upper levels SWNTs from the ground plane, as shown in Figure 5. Quantum capacitance (C_Q) arises as $4C_Q$ due to fourfold band degeneracy structure of

SWNT [4]. The values of C_E and C_Q are nearly same in magnitude. C_Q of all metallic SWNTs are oriented in parallel and then is series with C_E . Therefore, C_Q can be neglected for large value of N . The resistance and inductance of all metallic SWNTs are in parallel in bundle and N times smaller than that of a SWNT.

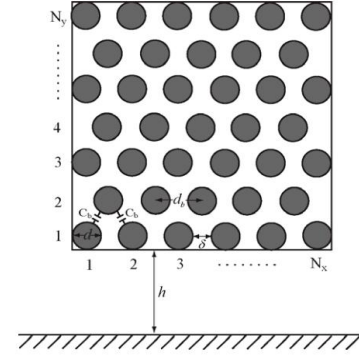


Fig 4: Cross-section of a SWNT bundle interconnects [27].

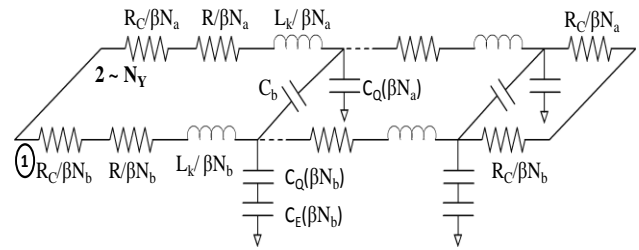


Fig 5: Equivalent circuit of a SWNT bundle interconnects [27].

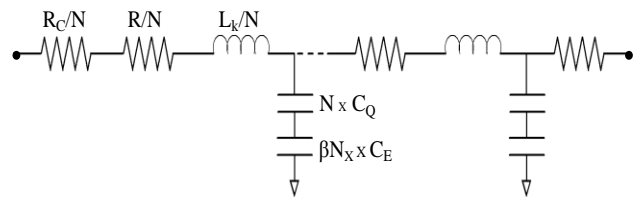


Fig 6: Simplified equivalent circuit of a SWNT bundle interconnects [27].

3. SIMULATION SETUP

In this paper, propagation delay for bundled SWNT and MWNT is measured at different interconnect lengths of 100, 200, 500, 1000 and 2000 μm [39] by using the geometries suggested in [26, 27, 40]. Simulation setup uses CMOS inverter at 32 nm technology node for which the technology parameters (length and width) of NMOS is taken as 32 nm and 640 nm and for PMOS, these parameters are taken as 32 nm and 1280 nm, respectively. As shown in Figure 7 and Figure 8, the input rise time is triggered at 90% whereas the output fall time is target at 10%. The delay is analyzed for different number of shells in MWNTs and for different number of SWNTs in the bundle. For each type of MWNT shells and SWNT bundles, the propagation

delay is measured for 20 distributed elements at different interconnect lengths.

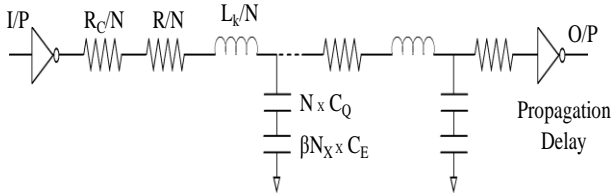


Fig 7: Simulation setup for SWNT Bundle interconnects [40]

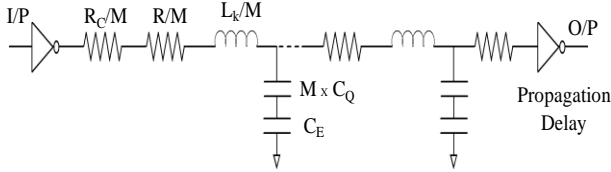


Fig 8: Simulation setup for MWNT interconnects [40]

4. RESULTS AND DISCUSSIONS

In this paper, HSPICE simulations are run for different number of shells in MWNTs and SWNTs in bundles at different global interconnect lengths to analyze the propagation delay. Figure 9 plots propagation delay at different interconnect lengths for fixed numbers of shells in MWNTs. Figure 11 shows variation of propagation delay for different number of shells in MWNTs at different interconnect lengths (global). Similar analysis is also carried out for SWNT bundle. For bundled SWNTs, Figures 10 and 12 represents variation of propagation delay at different interconnect lengths and at different numbers of SWNTs in bundle. This analysis is done for specified numbers of SWNTs in bundle and interconnects lengths (global), respectively. It can be interpreted that for both MWNT and bundled SWNT, propagation delay increases with increase in interconnect lengths. However, delay decreases with increasing number of shells and number of SWNTs in a bundle, respectively. A comparative analysis has also been done between number of shells in MWNTs and number of SWNTs in bundle. The global interconnect lengths are specified at 100, 200, 500, 1000 and 2000µm [39].

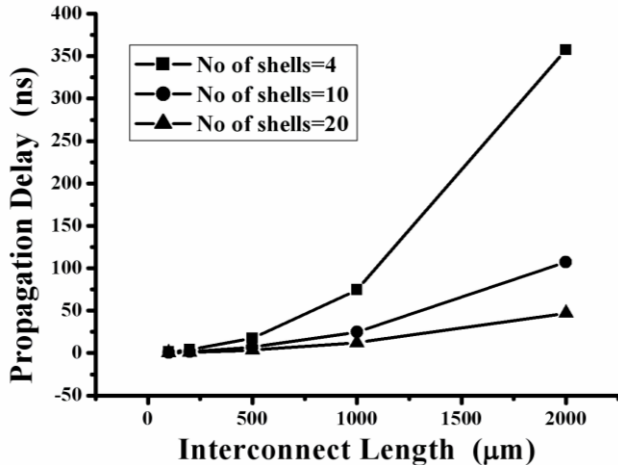


Fig 9: Propagation delays of MWNTs at different interconnect lengths (global) for varying numbers of shells

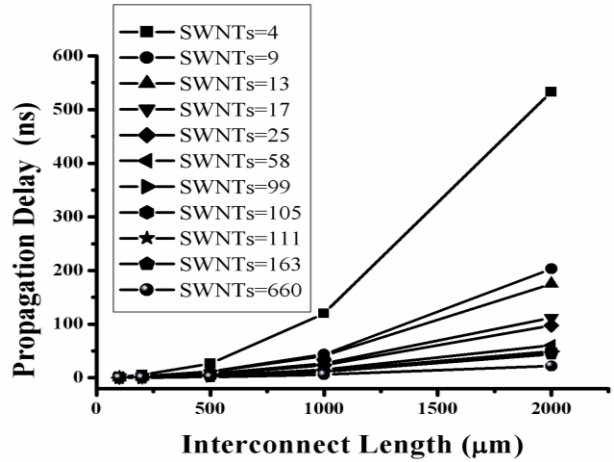


Fig 10: Propagation delay of SWNT bundle with varying interconnects lengths (global)

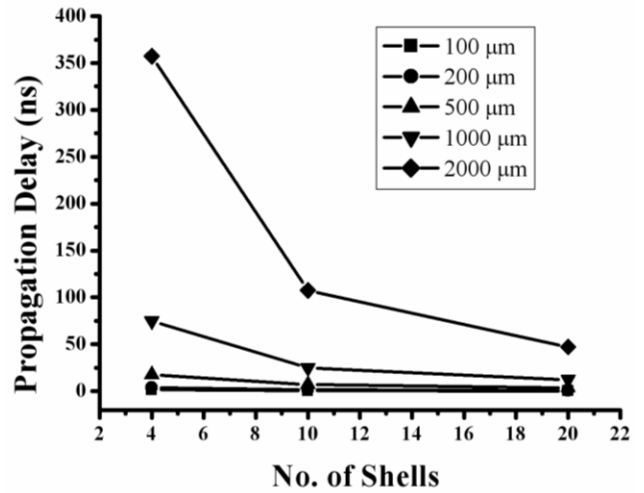


Fig 11: MWNT propagation delay with varying number of shells at different interconnect lengths (global)

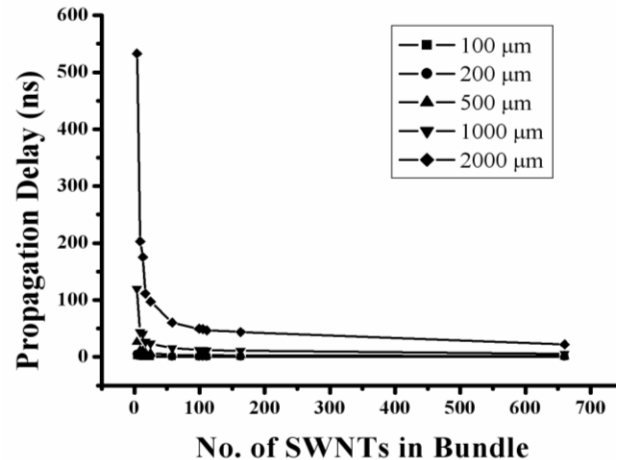


Fig 12: Propagation delays with varying number of SWNTs in bundle at different interconnect lengths (global)

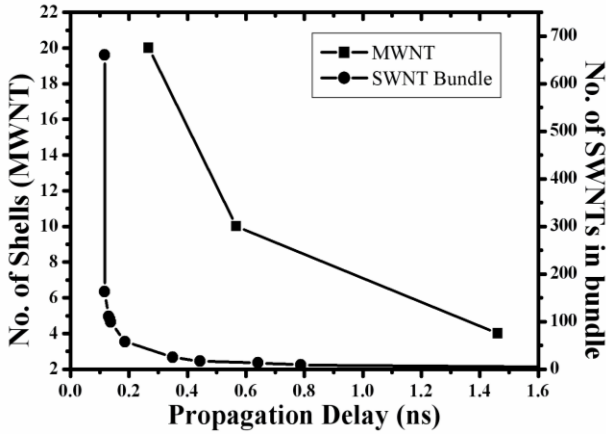


Fig 13: Equivalent number of shells in MWNTs with varying number of SWNTs in bundle at specified interconnect length of 100µm for same performance of propagation delay

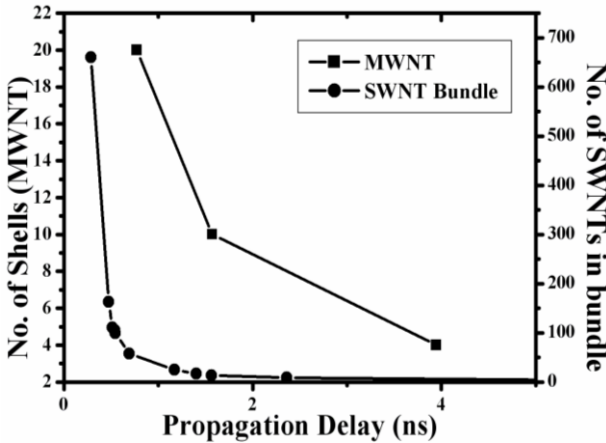


Fig 14: Equivalent number of shells in MWNTs with varying number of SWNTs in bundle at specified interconnect length of 200µm for same performance of propagation delay

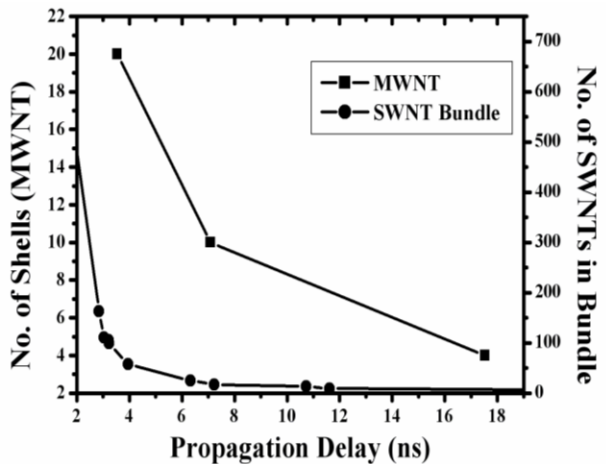


Fig 15: Equivalent number of shells in MWNTs with varying number of SWNTs in bundle at specified interconnect length of 500µm for same performance of propagation delay

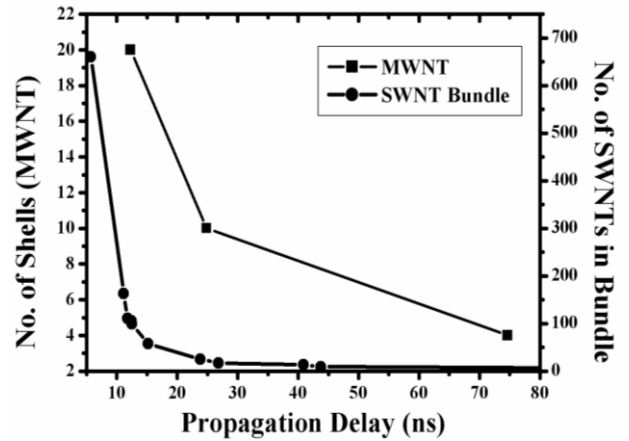


Fig 16: Equivalent number of shells in MWNTs with varying number of SWNTs in bundle at specified interconnect length of 1000µm for same performance of propagation delay

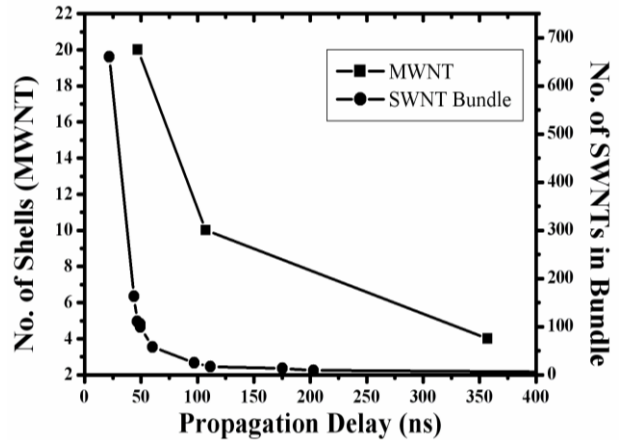


Fig 17: Equivalent number of shells in MWNTs with varying number of SWNTs in bundle at specified interconnect length of 2000µm for same performance of propagation delay

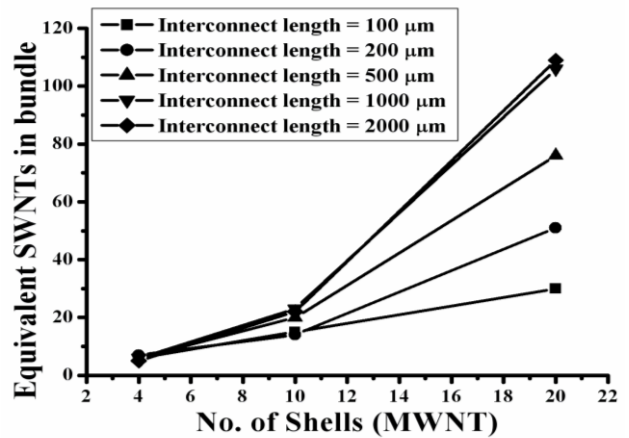


Fig 18: Equivalent number of SWNTs in the bundle for fixed numbers of shells in MWNTs at different interconnect lengths (global) for same performance of propagation delay

Figures 13, 14, 15, 16 and 17 graphically shows the analysis of propagation delay at different interconnect lengths for different number of shells in MWNTs and SWNTs in bundles. Finally, Figure 18 presents different numbers of SWNTs in bundle for fixed numbers of shells in MWNTs at specified interconnect lengths which is further approximated in Table 1. Table 1 suggests that at specified interconnect lengths (global), number of SWNTs in bundle is more than number of shells in MWNTs for same performance of propagation delay.

Table 1. Number of Shells (MWNTs) for Equivalent Number of SWNTs in Bundle at Different Interconnect Lengths (Global) for Same Performance of Propagation Delay

Interconnect Length	MWNT Shell = 4	MWNT Shell = 10	MWNT Shell = 20
100 μm	SWNTs = 5	SWNTs = 14	SWNTs = 30
200 μm	SWNTs = 6	SWNTs = 15	SWNTs = 51
500 μm	SWNTs = 6	SWNTs = 20	SWNTs = 76
1000 μm	SWNTs = 6	SWNTs = 22	SWNTs = 106
2000 μm	SWNTs = 7	SWNTs = 23	SWNTs = 109

The area is analyzed for equivalent number of shells in MWNTs and number of SWNTs in the bundle (Figure 19) in terms of diameters of SWNT bundle and MWNT. The areas of MWNTs depend on the number of shells and innermost and outermost diameters which is obtained by using equation (1). From this graphical analysis, it is clear that the area is minimized for equivalent shells of MWNTs than the equivalent number of SWNTs in bundle.

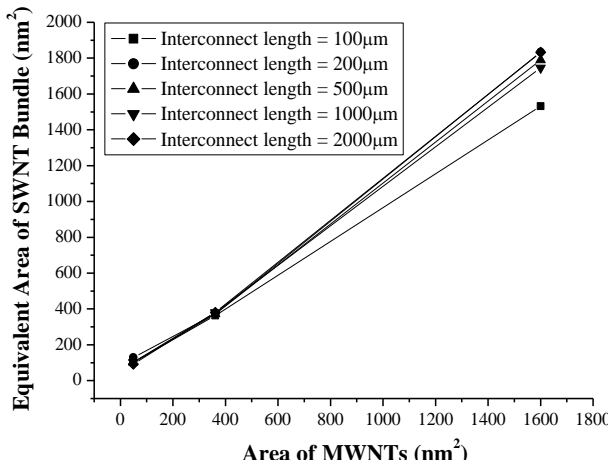


Fig 19: Equivalent area for different number of shells in MWNTs with varying number of SWNTs in bundle at different interconnect lengths (global)

5. CONCLUSION

In this paper, models for MWNT and SWNT bundle interconnects are reviewed on the basis of one-dimensional fluid theory. These models are compared at 32 nm technology nodes in terms of propagation delay and area. Simulation result shows that MWNT requires lesser area than SWNT bundle at different interconnect lengths for same performance of propagation delay. Therefore, for future VLSI technology, MWNTs may be proven as more promising candidate than copper.

6. REFERENCES

- [1] Goel, A. K. 2007. High-speed VLSI Interconnections. Wiley-IEEE Press.
- [2] Satio, R., Dresselhaus, G., and Dresselhaus, S. 1998. Physical Properties of Carbon Nanotubes. Imperial College Press. London, U. K.
- [3] Li, H., Xu, C., Srivastava, N., and Banerjee, K. 2009. Carbon Nanomaterials for Next-Generation Interconnects and Passives: Physics, Status and Prospects. IEEE Trans. Electron Devices. Res. 56, No. 9 (Sep. 2009), 1799-1821.
- [4] Javey, A. and Kong, J. 2009. Carbon Nanotube Electronics. Springer.
- [5] Wei, B. Q., Vajtai, R. and Ajayan, P. M. 2001. Reliability and current carrying capacity of carbon nanotubes. Appl. Phys. Lett., Res. 79, No. 8 (2001), 1172-1174.
- [6] Collins, P. G., Hersam, M., Arnold, M., Martel, R. and Avouris, P. 2001. Current saturation and electrical breakdown in multiwalled carbon nanotubes. Phys. Rev. Lett., Res. 86, No. 14 (2001), 3128-3131.
- [7] Berber, S., Kwon, Y. -K. and Tomanek, D. 2000. Unusually high thermal conductivity of carbon nanotubes. Phys. Rev. Lett., Res. 84, No. 20 (2000), 4613-4616.
- [8] Avouris, P., Chen, Z. and Perebeions, V. 2007. Carbon-based electronics. Nat. Nanotechnology. Res. 2, No. 10 (Oct. 2007), 605-613.
- [9] Tsukagoshi, K., Alphenaar, B. W. and Ago, H. 1999. Coherent transport of electron spin in a ferromagnetically contacted carbon nanotube. Nature. Res. 401, No. 6753 (Oct. 1999), 572-574.
- [10] Misewich, J. A., Martel, R., Avouris, P., Tsang, J. C., Heinze, S. and Tersoff, J. 2003. Electrically induced optical emission from a carbon nanotube FET. Science. Res. 300, No. 5620 (May 2003), 783-786.
- [11] Wang, N., Tang, Z. K., Li, G. D. and Chen, J. S. 2000. Materials science: Single-walled 4 Å carbon nanotube arrays. Nature. Res. 408, No. 6808 (Nov. 2000), 50-51.
- [12] Yu, M. F., Lourie, O., Dyer, M. J., Moloni, K., Kelly, T. F. and Ruoff, R. S. 2000. Strength and breaking mechanism of multiwalled carbon nanotubes under tensile load. Science. Res. 287, No. 5453 (Jan. 2000), 637-640.
- [13] Lu, F., Gu, L., Meziani, M. J., Wang, X., Luo, P. G., Veca, L. M., Cao, L. and Sun, Y. P. 2009. Advances in bioapplications of carbon nanotubes. J. Adv. Mater. Res. 21, No. 2 (2009), 139-152.
- [14] Du, C., Yeh, J. and Pan, N. 2005. High power density supercapacitors using locally aligned carbon nanotube

- electrodes. *J. Nanotechnology. Res.* 16, No. 4 (Feb. 2005), 350–353.
- [15] Wei, P., Bao, W., Pu, Y., Lau, C. N. and Shi, J. 2009. Anomalous thermoelectric transport of Dirac particles in graphene. *Phys. Rev. Letter. Res.* 102, No. 16 (Apr. 2009), 166 808.
- [16] Ago, H., Petritsch, K., Shaffer, M. S. P., Windle, A. H. and Friend R. H. 1999. Composites of carbon nanotubes and conjugated polymers for photovoltaic devices. *J. Adv. Matter. Res.* 11, No. 15 (1999), 1281–1285.
- [17] Choi, W. B., Chung, D. S., Kang, J. H., Kim, H. Y., Jin, Y. W., Han, I. T., Lee, Y. H., Jung, J. E., Lee, N. S., Park, G. S. and Kim, J. M. 1999. Fully sealed, high-brightness carbon-nanotube field-emission display. *Appl. Phys. Letter, Res.* 75, No. 20 (Nov. 1999), 3129–3131.
- [18] Collins, P. G., Arnold, M. S. and Avouris P. 2001. Engineering carbon nanotubes and nanotube circuits using electrical breakdown. *Science. Res.* 292, No. 5517 (Apr. 2001), 706–709.
- [19] Dadgour, H., Cassell, A. M. and Banerjee, K. 2008. Scaling and variability analysis of CNT-based NEMS devices and circuits with implications for process design. In *Proceedings of the IEEE International Electron Devices Meeting*, 529-53.
- [20] Hyperion Catalysis. [Online]. Available: <http://www.fibrils.com>.
- [21] Kreupl, F., Graham, A. P., Duesberg, G. S., Steinhogel, W., Liebau, M., Unger, E. and Honlein, W. 2002. Carbon nanotubes in interconnect applications. *J. Microelectronics Engg. Res.* 64, No. 1–4 (Oct. 2002), 399–408.
- [22] Li, J., Ye, Q., Cassell, A., Ng, H. T., Stevens, R., Han, J. and Meyyappan, M. 2003. Bottom-up approach for carbon nanotube interconnects. *Appl. Phys. Letter. Res.* 82, No. 15 (Apr. 2003), 2491–2493.
- [23] Li, H. and Banerjee, K. 2008. High-frequency effects in carbon nanotube interconnects and implications for on-chip inductor design. In *Proceedings of the IEEE International Electron Devices Meeting*, 525–528.
- [24] McEuen, L., Fuhrer, M. S. and Park, H. 2002. Single-walled Carbon Nanotube Electronics. *IEEE Trans. Nanotechnology. Res.* 1, No. 1 (Mar. 2002), 78-85.
- [25] Srivastava, N. and Banerjee, K. 2005. Performance Analysis of Carbon Nanotube Interconnects for VLSI Applications. In *Proceedings of the IEEE/ACM International Conference on Computer-aided design*.
- [26] Xu, Y. and Srivastava, A. 2009. A Model of Multi-Walled Carbon Nanotube Interconnects. In *Proceedings of the 52nd IEEE International Midwest Symposium on Circuits and Systems*.
- [27] Srivastava, A., Xu, Y. and Sharma, A. K. 2010. Carbon nanotubes for next generation very large scale integration interconnects. *J. Nanophotonics. Res.* 4, No. 041690 (May 2010), 1-26.
- [28] Xu, Y. and Srivastava, A. 2009. A model for carbon nanotube interconnects. *Int. J. Circuit Theory Appl. Res.* 38 (Mar. 2009), 559-575.
- [29] Burke, P. J. 2002. Luttinger Liquid Theory as a Model of the Gigahertz Electrical Properties of Carbon Nanotubes. *IEEE Trans. Nanotechnology. Res.* 1, No. 3 (Sep. 2002), 129-144.
- [30] Miano, G. and Villone, F. 2006. An integral formulation for the electrodynamic of metallic carbon nanotubes based on a fluid model. *IEEE Trans. Antennas and Propagations. Res.* 54, No. 10 (2006), 2713-2724.
- [31] Nihei, M., Kondo, D., Kawabata, A., Sato, S., Shioya, H., Sakae, M., Iwai, T., Ohfuti, M. and Awano, Y. 2005. Low-resistance multi-walled carbon nanotube vias with parallel channel conduction of inner shells. In *Proceedings of the IEEE International Tech. Conference*, 234-236.
- [32] Li, H. J., Lu, W. G., Li, J. J., Bai, X. D. and Gu, C. Z. 2005. Multichannel ballistic transport in multiwall carbon nanotubes. *Phys. Rev. Lett. Res.* 95, No. 8 (Aug. 2005).
- [33] Yan, Q., Wu, J., Zhou, G., Duan, W. and Gu, B. –L. 2005. Ab initio study of transport properties of multiwalled carbon nanotubes. *Physical review B, Res.* 72, No. 15 (Oct. 2005), 155425-1 – 155425-5.
- [34] Naeemi, A. and Meindl, J. D. 2006. Compact physical models for multiwall carbon nanotube interconnects. *IEEE Electron Devices Lett. Res.* 27, No. 5 (May 2006), 338-340.
- [35] Nieuwoudt, A. and Massoud, Y. 2006. Understanding the Impact of Inductance in Carbon Nanotube Bundles for VLSI Interconnect Using Scalable Modeling Techniques. *IEEE Trans. Nanotechnology. Res.* 5, No. 6 (Nov. 2006).
- [36] Xu, Y., Srivastava, A. and Sharma, A. K. 2010. Emerging Carbon Nanotube Electronic Circuits. *J. VLSI Design, Res.* 2010 (2010), 1-8.
- [37] Peng, N., Zhang, Q., Li, J. and Liu, N. 2006. Influences of ac electric field on the spatial distribution of carbon nanotubes formed between electrodes. *J. Appl. Physics, Res.* 100, No. 2 (Jul. 2006), 024309-1 – 024309-5.
- [38] Zheng, M., Jagota, A.M., Strano, S., Santos, A. P., Barone, P., Chou, S. G., Diner, B. A., Dresselhaus, M. S., McLean, R. S., Onoa, G. B., Samsonidze, G. G., Semke, E. D., Usrey, M. and Walls, D. J. 2003. Structure-based carbon nanotube sorting by sequence dependent DNA assembly. *Science. Res.* 302, No. 5650 (Nov. 2003), 1545–1548.
- [39] Alam, N., Kureshi, A. K., Hasan, M. and Arslan, T. 2009. Carbon Nanotube Interconnects for Low-Power High-Speed Applications. In *Proceedings of the IEEE International Symposium on Circuits and Systems*, 2273–2276.
- [40] Majumder, M. K., Kaushik, B. K. and Manhas, S. K. 2011. Performance Comparison between Single wall Carbon Nanotube Bundle and Multiwall Carbon Nanotube for Global Interconnects. In *Proceedings of the IEEE International Conference on Networks and Computer Communications (ETNCC), Udaipur, Rajasthan*, 104-109.